A Computational Study on the Decomposition of Formic Acid Catalyzed by $(H_2O)_x$, $x = 0-3$: Comparison of the Gas-Phase and Aqueous-Phase Results

Hsin-Tsung Chen,*,† Jee-Gong Chang,*,† and Hui-Lung Chen*,‡

National Center for High-Performance Computing, No. 28, Nan-Ke Third Road, Hsin-Shi, Tainan 74147, Taiwan, and Cherry L. Emerson Center for Scientific Computation and Department of Chemistry, Emory University, Atlanta, Georgia 30322

Received: February 12, 2008; Revised Manuscript Received: May 5, 2008

The mechanisms for the water-catalyzed decomposition of formic acid in the gas phase and aqueous phase have been studied by the high-level G2M method. Water plays an important role in the reduction of activation energies on both dehydration and decarboxylation. It was found that the dehydration is the main channel in the gas phase without any water, while the decarboxylation becomes the dominant one with water catalyzed in the gas phase and aqueous phase. The kinetics has been studied by the microcanonical RRKM in the temperature range of 200−2000 K. The predicted rate constant for the $(H_2O)_3$-catalyzed decarboxylation in the aqueous phase is in good agreement with the experimental data. The calculated CO_2/CO ratio is 200−74 between 600−700 K and 178−303 atm, which is consistent with the average ratio of 121 measured experimentally by Yu and Savage (ref 3).

Introduction

Carboxylic acids such as formic acid are an important intermediate in the oxidation of organic hydrocarbons in both atmospheric chemistry[1] and aqueous phases.[2,3] It is well-known that there are two reaction channels in the decomposition of formic acid: (1) dehydration and (2) decarboxylation.

$$HCOOH \rightarrow H_2O + CO \quad (1)$$

$$\rightarrow CO_2 + H_2 \quad (2)$$

Many studies on the unimolecular decomposition of formic acid in the gas phase have been reported both experimentally[4–7] and theoretically.[8–12] In the gas phase, the dehydration starting from *Z*-conformer formic acid is the main dissociation channel, whereas the decarboxylation starting from *E*-conformer formic acid is less competitive. The measured activation energies (E_a)[4–7] of dehydration and decarboxylation are in a wide range: the E_a values of dehydration and decarboxylation are 32−66 and 48−68 kcal/mol, respectively. Only the highest E_a values of experiments are supported by the high-level calculations.[8,9,11–14] In contrast, the decarboxylation reaction becomes more significant in the aqueous-phase experiments.[3,15,16] To explain the difference between the gas and aqueous phases, water as a homogeneous catalyst has been studied by several theoretical researchers.[11,12,14,17,18] Ruelle et al.[10,11] showed that using water as a catalyst reduces the activation barrier of the decarboxylation reaction. Later, Melius et al.,[14] Akiya et al.,[19] and Wang et al.[12] studied the effect of water on both dehydration and decarboxylation and illustrated those pathways are catalyzed by water. Particularly, the barrier height of the decarboxylation decreases dramatically and becomes the favored channel.

As presented above, many investigations for the decomposition of formic acid with and without water catalyzed in the gas phase have been performed. However, there have been no high-level ab initio studies on the mechanisms in the aqueous conditions. In the present, we report the water-catalyzed decomposition mechanisms of formic acid in the gas phase and aqueous phase by the high-level G2M method. We carry out the polarizable continuum model (PCM)[20,21] in water solution for the aqueous phase. Accordingly, we also predict the rate constants for decomposition of formic acid in the aqueous conditions. The results are presented in the following sections in detail.

Computational Methods

The optimized geometries of the reactants, intermediates, transition states, and products for the formic acid decomposition in the gas phase and aqueous phase have been calculated at the B3LYP/6-311+G(3df, 2p) level.[22–24] The vibrational frequencies were calculated at this level for characterization of stationary points' zero-point energy (ZPE) corrections. To obtain more reliable values of energies for PES and rate constant predictions, we performed a series of single-point energy calculations for each stationary points with the modified Gaussian-2 method, G2M(CC1) scheme,[25] based on the optimized geometries at the B3LYP/6-311+G(3df, 2p) level. The G2M(CC1) composite scheme is given as follows:

$$E[\text{G2M(CC1)}] = E_{bas} + \Delta E(+) + \Delta E(2df) + \Delta E(CC) + \Delta + \Delta E(HLC, CC1) + ZPE$$

where

$$E_{bas} = E[\text{PMP4/6-311G(d, p)}]$$

$$\Delta E(+) = E[\text{PMP4/6-311 + G(d, p)}] - E_{bas}$$

$$\Delta E(2df) = E[\text{PMP4/6-311 + G(2df, p)}] - E_{bas}$$

$$\Delta E(CC) = E[\text{CCSD(T)/6-311 + G(d, p)}] - E_{bas}$$

$$\Delta = E[\text{PMP2/6-311 + G(3df, p)}] - E[\text{PMP2/6-311 + G(2df, p)}] - E[\text{PMP2/6-311 + G(d, p)}] + E[\text{PMP2/6-311G(d, p)}]$$

* Corresponding author. E-mail: bpett.tw@yahoo.com.tw (H.-T.C.); changjg@nchc.org.tw (J.-G.C.); hlchen@euch4e.chem.emory.edu (H.-L.C.).
† National Center for High-Performance Computing.
‡ Emory University.

10.1021/jp801247d CCC: $40.75
Published on Web 08/08/2008

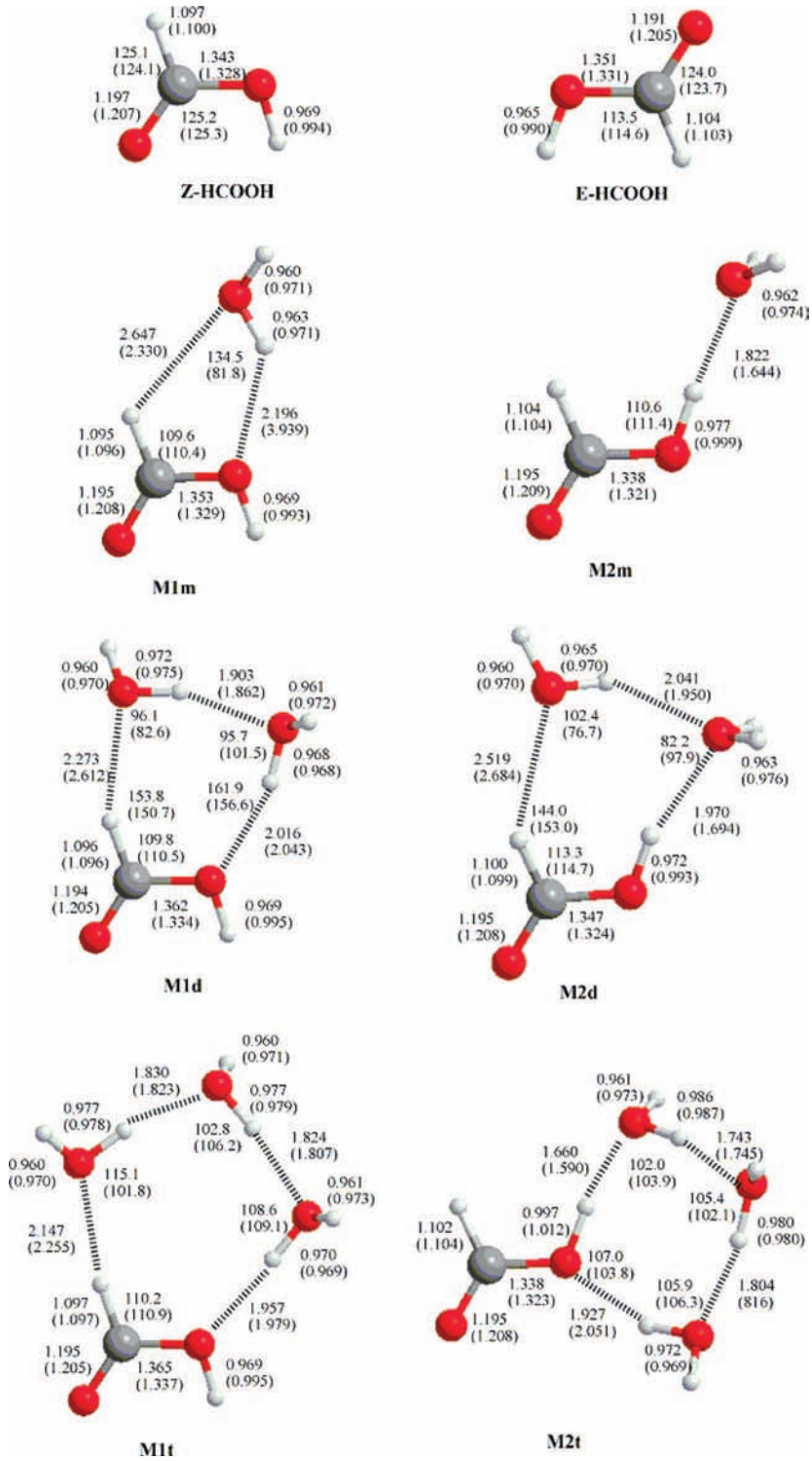

Figure 1. The optimized geometries of the intermediates of the decomposition of formic acid calculated in the gas phase and aqueous phase at the B3LYP/6-311+G (3df, 2p) level. The values in parentheses are calculated by PCM for the aqueous phase.

The higher level correction ΔE(HLC, CC1) is given by $-5.77n_\beta - 0.19n_\alpha$ in millihartree, where n_α and n_β are the numbers of α and β valence electrons, respectively.

For the aqueous-phase calculations, the polarizable continuum model (PCM)[20,21] as implemented in Gaussian 03 was used to account for the continuum solvation effects. The united atom for Hartree−Fock (UAHF) model was used to build the cavity in PCM, denoted as PCM/UAHF. Water with a dielectric constant of 78 was selected to represent a highly polar condensed-phase medium. All calculations have been carried out using the Gaussian 03 program package.[26]

Results and Discussion

The calculated geometries of the intermediates and transition states for decomposition of formic acid in the gas phase and aqueous phase at B3LYP/6-311+G (3df, 2p) are summarized in Figures 1 and 2, respectively. Figures 3 and 4 present the potential energy surface decomposition of formic acid in the gas phase and aqueous phase (PCM calculations) at G2M level, respectively. In these figures, bond distances are given in angstroms, angles in degrees, and energies in kcal/mol, respectively. A comparison with previous studies of barrier heights

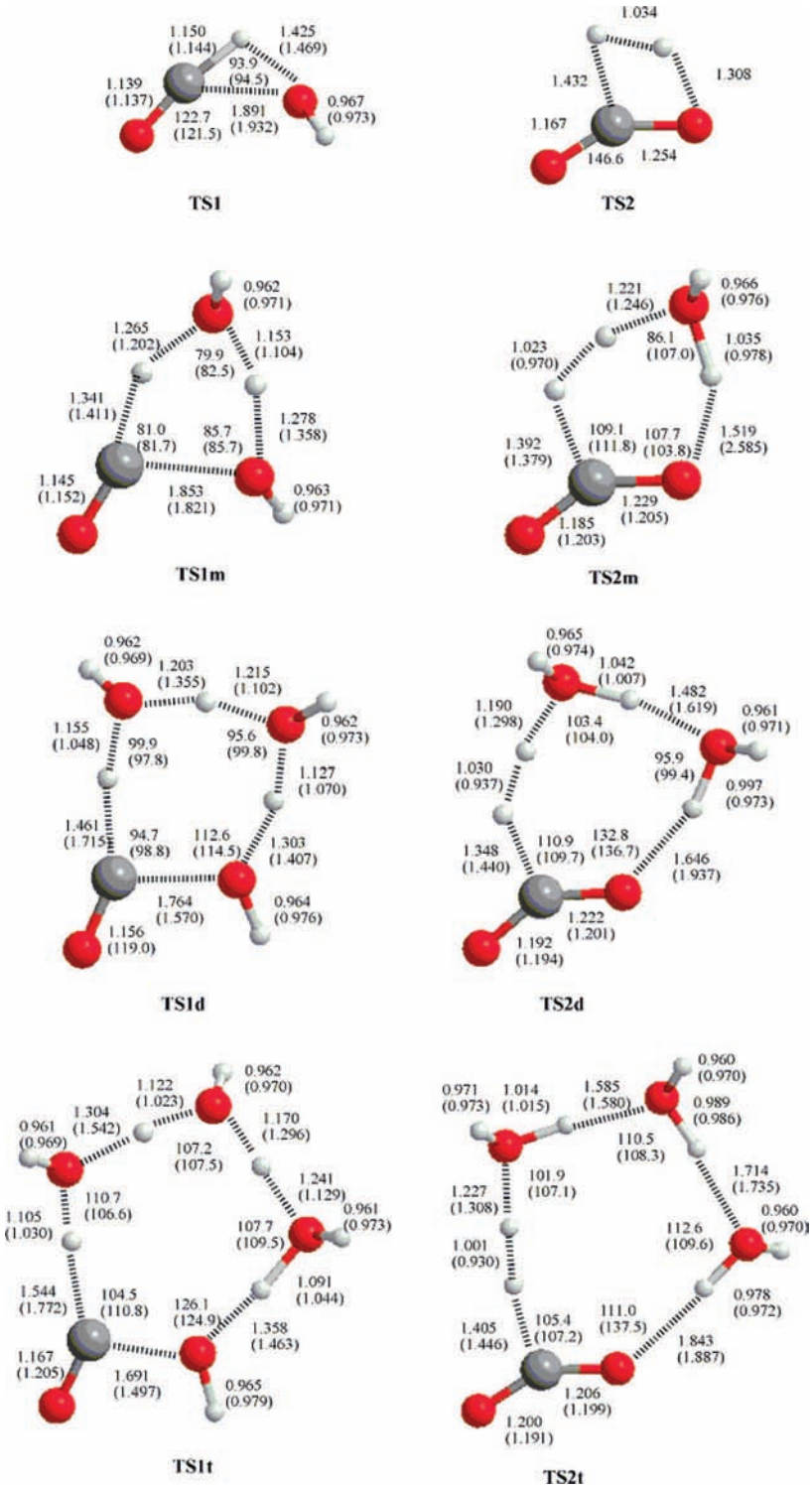

Figure 2. The optimized geometries of the transition states of the decomposition of formic acid calculated in the gas phase and aqueous phase at the B3LYP/6-311+G (3df, 2p) level. The values in parentheses are calculated by PCM for the aqueous phase.

for the dehydration and decarboxylation decomposition in the gas phase and aqueous phase is compiled in Table 1. In the present calculations, four models are assumed in the gas and aqueous phases: (A) unimolecular, (B) H_2O-catalyzed, (C) $(H_2O)_2$-catalyzed, and (D) $(H_2O)_3$-catalyzed. The mechanisms are presented in the following sections in detail.

1. Decomposition of Formic Acid in Gas Phase. ***A. Unimolecular.*** As shown as Figure 3, the heat of reaction and barrier height of the *Z*-HCOOH → *E*-HCOOH isomerization are predicted to be 3.9 and 11.3 kcal/mol, which are in good agreement with the experimental values[27,28] of 3.9 and 10.9 kcal/mol, respectively. In the dehydration starting from *Z*-HCOOH, it occurs by a concerted step passing a three-centered ring transition state, TS1, to produce H_2O + CO over a 67.4 kcal/mol barrier. From *E*-HCOOH, the decarboxylation first takes place via a four-centered transition state TS2 to generate CO_2 and H_2 with a barrier height of 65.9 kcal/mol. The calculated barriers of the favored dehydration and decarboxylation are 67.4 and 69.8 kcal/mol, which are in good agreement with the experimental data of 62−65 and 65−67 kcal/mol, respectively

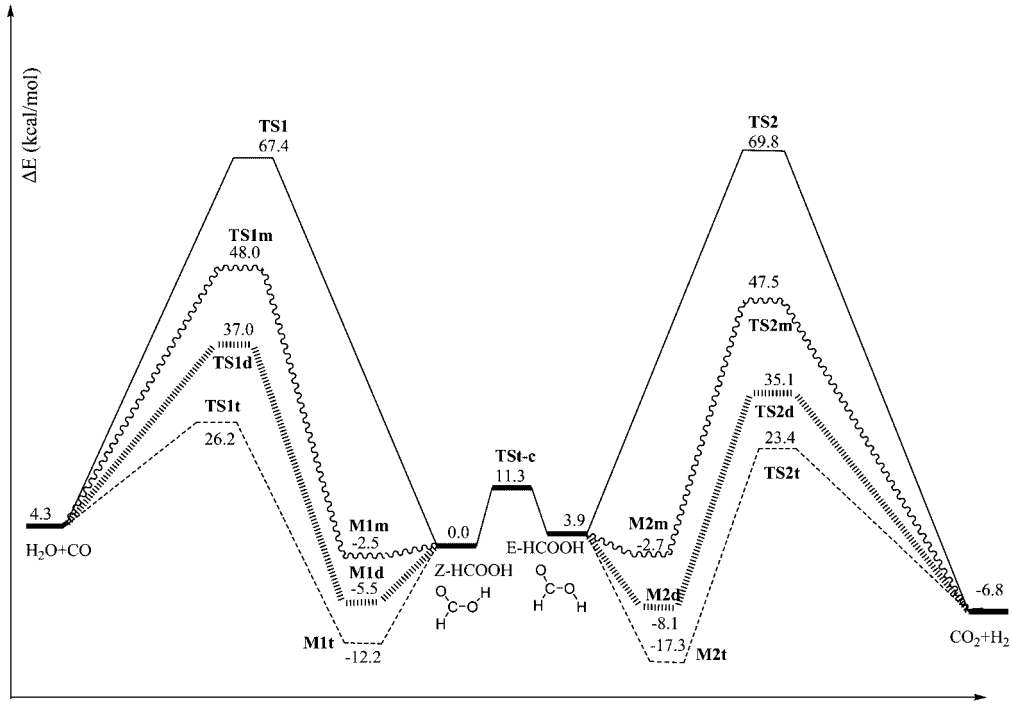

Figure 3. Schematic energy diagram for the decomposition reaction of formic acid in gas phase calculated at the G2M(CC1)//B3LYP/6-311+G (3df, 2p) level, where energy is given in kcal/mol.

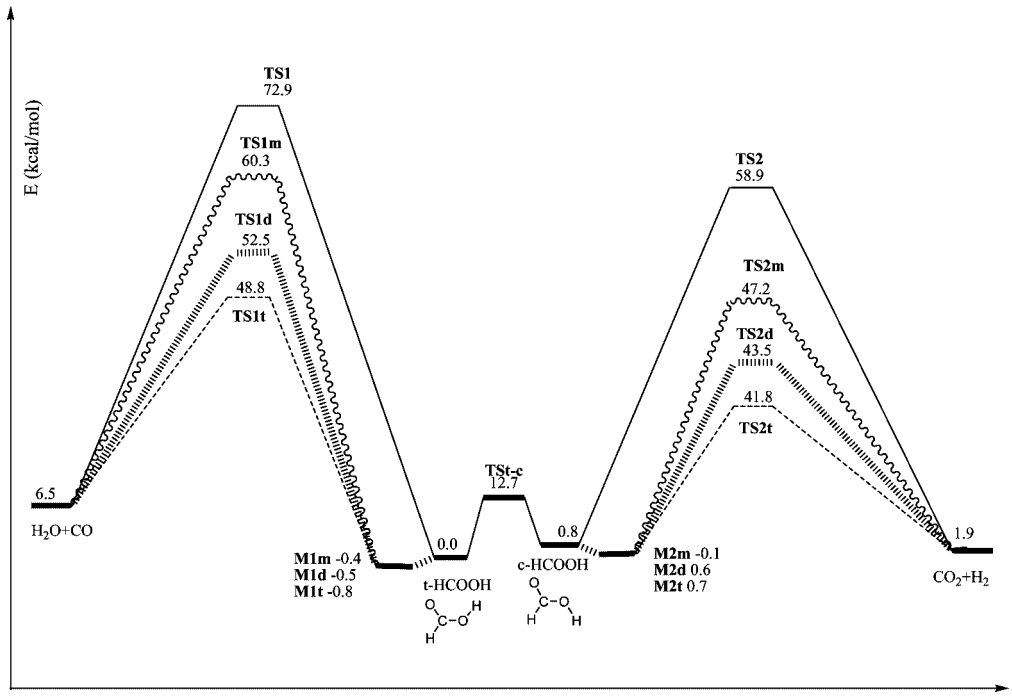

Figure 4. Schematic energy diagram for the decomposition reaction of formic acid in aqueous phase calculated by PCM at the G2M(CC1)// B3LYP/6-311+G (3df, 2p) level, where energy is given in kcal/mol.

(see Table 1). Our G2M (CC1) results are also in good agreement with high level calculations listed in Table 1.

B. H_2O-Catalyzed. The role of water is as a catalyst and simultaneously as a proton donor and acceptor, which makes the hydrogen-bond network ring with the formic acid. As shown in Figure 3, the H_2O-catalyzed reaction starts by the formation of the intermediates M1m and M2m. In M1m (see Figure 2), *Z*-HCOOH and H_2O are combined with two hydrogens bonding, while M2m involves *E*-HCOOH and H_2O with only one hydrogen bonding. The H-bond $OH_{formic\ acid}\cdots O_{water}$ of M2m is 0.374 Å shorter than the H-bond $O_{water}\cdots HO_{formic\ acid}$ of M1m. This result corresponds with the binding energy D_o of intermediates M1m and M2m; the binding energy of M2m is 0.2 kcal/mol larger than that of M1m. It is inconsistent with the unimolecular HCOOH reaction that *Z*-HCOOH is more stable than *E*-HCOOH. From M1m, the process undergoes a dehydration process, producing $2H_2O + CO$ by the transition state TS1m. TS1m shows a two hydrogen transfer process as a five-centered ring, shown in Figure 2. At TS1m, the breaking bond of C−O is simultaneous with hydrogen transfer from C to O_{water} and from O_{water} to $O_{formic\ acid}$. The breaking bond of C−O is 1.853 Å. The decarboxylation process stars from M2m to form

TABLE 1: Comparison of the Calculated Activation Energies of the Unimolecular and Water-Catalyzed Decomposition of Formic Acid in the Gas Phase and Aqueous Phase with Previous Studies

reactions	this work	theoretical studies	experimental
		Dehydration	
unimolecular	67.4	67.5 (MP4SDTQ/6-31**//MP2/6-31G**)[a]	60.5[f]
	(72.9)[k]	70.1 (BAC-MP4 method)[b]	62−65[g]
		63.0 (PMP4/6-311++G**//UMP2/6-311G**)[c]	
		68 (DZ + P CCSDT- l//DZ + P CCSD)[d]	
		64.6 (B3LYP/6-311++G(3df, 3pd))[e]	
H_2O-catalyzed	48.0	44.0 (BAC-MP4 method)[b]	
	(60.3)[k]	45.5 (B3LYP/6-311++G(3df, 3pd))[e]	
$(H_2O)_2$-catalyzed	37.0	27.7 (BAC-MP4 method)[b]	
	(52.5)[k]	34.7 (B3LYP/6-311++G(3df, 3pd))[e]	
$(H_2O)_3$-catalyzed	26.2		
	(48.8)[k]		
		Decarboxylation	
unimolecular	69.8	64.9 (BAC-MP4 method)[b]	65−68[g]
	(58.9)[k]	65.2 (PMP4/6-311++G**//UMP2/6-311G**)[c]	
		71 (DZ + P CCSDT- l//DZ + P CCSD)[d]	
		66.6 (B3LYP/6-311++G(3df, 3pd))[e]	
H_2O-catalyzed	47.5	48.7 (MP4SDTQ/6-31**//MP2/6-31G**)[a]	
	(47.2)[k]	37.3 (BAC-MP4 method)[b]	
		41.6 (B3LYP/6-311++G(3df, 3pd))[e]	
$(H_2O)_2$-catalyzed	35.1	21.5 (BAC-MP4 method)[b]	
	(43.5)[k]	32.5 (B3LYP/6-311++G(3df, 3pd))[e]	
$(H_2O)_3$-catalyzed	23.4		
	(41.8)[k]		
		Decarboxylation	
water-catalyzed			25.3[h]
water-catalyzed			33.6 ± 17.2[i]

[a] Reference 11. [b] Reference 14. [c] Reference 8. [d] Reference 9. [e] Reference 12. [f] Reference 4. [g] Reference 5. [h] Reference 16. [i] Reference 3. [k] The values in parentheses are calculated by PCM for the aqueous phase.

$CO_2 + H_2 + H_2O$ by the transition state TS2m. TS2m is a one hydrogen transfer process as a six-centered ring (see Figure 2). At TS2m, the forming bond of H−H is 1.023 Å, which is 0.280 Å longer than that of H_2. The barrier heights for the dehydration and decarboxylation reactions are 48.0 and 47.5 kcal/mol, respectively. As compared to the unimolecular reaction, the H_2O-catalyzed reaction is about 20 kcal/mol lower in barrier for both dehydration and decarboxylation reactions, respectively.

C. $(H_2O)_2$-Catalyzed. Similar to the H_2O-catalyzed reaction, the reaction starts by the formation of the intermediates M1d and M2d. M1d and M2d have seven-centered ring structures with three hydrogen-bonded complexes. The H-bond $CH_{formic\ acid}\cdots O_{water}$ of M1d is 0.246 Å shorter than the H-bond $O_{water}\cdots HC_{formic\ acid}$ of M2d. This result corresponds with the binding energy (D_o) that the D_o of M1d is 2.6 kcal/mol larger than that of M2d. The dehydration process from M1d produces $3H_2O + CO$ by the transition state TS1d. TS1d is a seven-centered ring containing a three hydrogen transfer process (see Figure 2). At TS1d, the breaking bond of C−O is 1.764 Å, which is slightly shorter than that in TS1m. The decarboxylation process starts from M2d to form $CO_2 + H_2 + 2H_2O$ by the transition state TS2d. TS2d is an eight-centered ring containing a two hydrogen transfer process (see Figure 2). At TS2m, the forming bond of H−H is 1.030 Å, which is 0.0287 Å longer than that of H_2. The barrier heights for the dehydration and decarboxylation reactions are 37.0 and 35.1 kcal/mol, respectively. The $(H_2O)_2$-catalyzed reaction is about 30.6 and 34.5 kcal/mol lower in barrier for both reactions.

D. $(H_2O)_3$-Catalyzed. M1t and M2t have nine-centered ring and eight-centered ring structures with four hydrogen-bonded complexes. M1t and M2t are more stable than the reactants due to forming more hydrogen bonds. The strong hydrogen bonds in M2t result in a binding energy D_o of M2t (17.3 kcal/mol) that is larger than that of M1t (12.2 kcal/mol). M1t undergoes a dehydration process, producing $4H_2O + CO$ by the transition state TS1t. TS1t is a nine-centered ring containing a four hydrogen transfer process, shown in Figure 2. The breaking bond of C−O is 1.691 Å, which is 0.162 Å shorter than that in TS1m. The decarboxylation process starts from M2t to from $CO_2 + H_2 + 3H_2O$ by the transition state TS2t. TS2t is a 10-centered ring containing a three hydrogen transfer process (see Figure 2). At TS2t, the forming bond of H−H is 1.001 Å, which is 0.022 Å shorter than that of TS2m. The barrier heights of Ts1t and TS2t for dehydration and decarboxylation reactions reduce to 26.2 and 23.4 kcal/mol, respectively.

As a result, the addition water molecules are significant for both dehydration and decarboxylation decomposition. However, the energy barrier of the decarboxylation is lower than that of dehydration by about 0.5−2.8 kcal/mol, suggesting decarboxylation becomes significant in the presence of water. As shown in Table 1, it is noticed that the energy barriers of TS2d and TS2t are in good agreement with experimental values of 33.6 ± 17.2 and 25.3 kcal/mol.[3,16] This result is consistent with the experimental observations[3,15,16] that decarboxylation is dominant under hydrothermal conditions.

2. Water Solvent: PCM Calculations. To demonstrate the difference in the selectivity in the gas phase and aqueous phase, we carried out PCM calculations with water as a solvent. This may allow one not only to simulate exact experimental conditions, but also to estimate the effect of the medium on the mechanism of the reaction in more detail and to make some predictions. In the PCM calculations, four models, as described above, are considered. All of the intermediates and transition states for decomposition of formic acid in PCM calculations are reoptimized at B3LYP/6-311+G (3df, 2p) level of theory and summarized in Figures 1 and 2, respectively (see the values

in the parentheses). All transition states are verified by the number of imaginary frequencies (NIMG) with NIMG = 1. The imaginary frequencies are 1463.4i, 538.8i, and 289.2i and 1239.0i, 1149.3i, and 1001.4i for TS1x and TS2x (x = m, d, and t), respectively. We are not able to locate TS2 in PCM calculation. Thus, the energy of TS2 is calculated on the basis of the optimized geometry in the gas phase. The PES of PCM calculations applied at the G2M//B3LYP/6-311+G(3df, 2p) optimized energy are presented in Figure 4. It is noticed that the relative energies of all intermediates including zero-, one-, two-, and three-water-molecular-coordinated species are smaller than 1.0 kcal/mol with respect to reactants (*Z*-HCOOH + $(H_2O)_{x=0-3}$). As shown in Figure 4, the barrier heights of the dehydration are 72.9, 60.3, 52.5, and 48.8 kcal/mol, while the barrier energies of the decarboxylation are 58.9, 47.2, 43.5, and 41.8 kcal/mol for unimolecular, H_2O-, $(H_2O)_2$-, and $(H_2O)_3$-catalyzed reactions, respectively. The barrier of the unimolecular decarboxylation is 14 kcal/mol lower than the dehydration in the aqueous phase (in PCM calculations), whereas the barrier of the unimolecular dehydration is 2.4 kcal/mol lower than the decarboxylation in the gas phase. As compared to the gas-phase system, the barriers for both pathways do not decrease dramatically, but the decarboxylation becomes the main channel. In PCM calculations, the barrier energy of the decarboxylation is much lower than that of dehydration by about 7−14 kcal/mol, indicating the decarboxylation becomes more significant in the aqueous phase. As shown in Table 1, it is worth noting that the energy barriers of decarboxylation reactions are also in good agreement with the experimental value of 33.6 ± 17.2 kcal/mol,[3] indicating that the decarboxylation is the dominant channel under hydrothermal conditions.

3. Rate Constant Calculation. The microcanonical Rice−Ramsperger−Kassel−Marcus (RRKM) theory[29−32] was employed to calculate the rate constants for the decomposition of formic acid reaction with three waters in the aqueous phase. The optimized formic acid−water complexes are almost the same as the sum of their individual reactants in energy; they can be regarded as single molecule entities. We treated the reaction as practically unimolecular in this study. The effect of quantum-mechanical tunneling has been considered (on the basis of the Eckart approach implemented in the ChemRate program[33]). All calculations were done in the temperature range 200−2000 K at high-pressure limit and low-pressure limit.

The calculated Arrhenius expressions for dehydration (k_1) and dehydrogenation (k_2) at high-pressure limit and low-pressure limit for the temperature range 200−2000 K are given as:

At high-pressure limit,

$$k_1^{\infty} = 4.97 \times 10^{10} \exp(-47.51 \text{ kcal mol}^{-1}/RT) \text{ s}^{-1}$$

$$k_2^{\infty} = 5.04 \times 10^{9} \exp(-38.13 \text{ kcal mol}^{-1}/RT) \text{ s}^{-1}$$

At low-pressure limit,

$$k_1^0 = 3.09 \times 10^{22}\, T^{-0.0068} \times \exp(-46.56 \text{ kcal mol}^{-1}/RT) \text{ cm}^3 \text{ mol}^{-1} \text{ s}^{-1}$$

$$k_2^0 = 3.77 \times 10^{21}\, T^{-0.0065} \times \exp(-39.30 \text{ kcal mol}^{-1}/RT) \text{ cm}^3 \text{ mol}^{-1} \text{ s}^{-1}$$

The predicted parameters of log A = 9.7 and E = 38.1 kcal/mol for the decarboxylation reaction are in good agreement with experimental values[19] of log A = 9.3 and E = 33.6 kcal/mol in the temperature range of 320−420 °C, respectively. Comparing the CO_2/CO ratios with the experimental values reported by Savage and co-workers,[19] the calculated values are between 200 and 74 at temperature of 600−700 K and pressure of 178−303 atm, which are in agreement with the average ratio of 121 measured experimentally[19] at a temperature of 380 °C and pressure range of 178−303 atm. In the previous study,[13] we have calculated the unimolecular decomposition kinetics of formic acid in the gas phase. The predicted rate constants for unimolecular dehydration and decarboxylation in the gas phase are given by $k_1^0 = 4.05 \times 10^{15} \exp(-52.98 \text{ kcal mol}^{-1}/RT)$ $\text{cm}^3 \text{ mol}^{-1} \text{ s}^{-1}$ and $k_2^0 = 1.69 \times 10^{15} \exp(-51.11 \text{ kcal mol}^{-1}/RT)$ $\text{cm}^3 \text{ mol}^{-1} \text{ s}^{-1}$, which are in good agreement with the experimental results.[5,6,34] The calculated CO/CO_2 ratio, 13.57−13.90, between 1300 and 2000 K, is in good agreement with the experimental ratio of 10 measured by Hsu et al.[5]

Conclusion

The decomposition mechanisms of formic acid by water catalyzed in the gas phase and aqueous phase have been studied by the high-level G2M method. Water behaves as a homogeneous catalyst, which reduces the activation energies for both dehydration and decarboxylation. Our results show that dehydration is the main pathway in the gas phase, while the decarboxylation becomes dominant in the water-catalyzed gas phase and aqueous phase. The predicted rate constant for the $(H_2O)_3$-catalyzed decarboxylation in the aqueous phase is in good agreement with the results of Savage and co-workers. The predicted parameters of log A = 9.7 and E = 38.1 kcal/mol for the decarboxylation reaction are consistent with the experimental values of log A = 9.3 and E = 33.6 kcal/mol, respectively. The calculated CO_2/CO ratios are 200−74 between 600 and 700 K and 178 and 303 atm, which are in agreement with the average ratio of 121 measured experimentally.

Acknowledgment. We gratefully acknowledge the financial support provided to this study by the National Science Council, Republic of China, under Grant No. NSC 96-2221-E-492-008 and the use of CPUs from the National Center for High-Performance Computing, Taiwan.

References and Notes

(1) Chameides, W. L.; Davis, D. D. *Nature* **1983**, *304*, 427.
(2) Mishra, V. S.; Mahajuni, V. V.; Joshi, J. B. *Ind. Eng. Chem. Res.* **1995**, *34*, 2.
(3) Yu, J.; Savage, P. E. *Ind. Eng. Chem. Res.* **1998**, *37*, 2.
(4) Black, P. G.; Davis, H. H.; Jackson, G. E. *J. Chem. Soc. B* **1971**, 1923.
(5) Hsu, D. S.; Shaub, W. M.; Blackbum, M.; Lin, M. C. Expt *The 19th International Symposium on Combustion*; The Combustion Institute: Pittsburgh, PA, 1983; p 89.
(6) Saito, K.; Kakamoto, T.; Kuroda, H.; Torii, S.; Imamura, A. *J. Chem. Phys.* **1984**, *80*, 4989.
(7) Samsonov, Y. N.; Petroy, A. K.; Baklanov, A. V.; Vihzin, V. V. *React. Kinet. Catal. Lett.* **1976**, *5*, 197.
(8) Francisco, J. S. *J. Chem. Phys.* **1992**, *96*, 1167.
(9) Goddard, J. D.; Yamaguchi, Y.; Schaefer, H. F., III *J. Chem. Phys.* **1992**, *96*, 1158.
(10) Ruelle, P. *J. Am. Chem. Soc.* **1987**, *109*, 1722.
(11) Ruelle, P.; Kesselring, U. W.; Nam-Tran, H. *J. Am. Chem. Soc.* **1986**, *108*, 371.
(12) Wang, B.; Hou, H.; Gu, Y. *J. Phys. Chem. A* **2000**, *104*, 10526.
(13) Chang, J.-G.; Chen, H.-T.; Xu, S.; Lin, M. C. *J. Phys. Chem. A* **2007**, *111*, 6789.
(14) Melius, C. F.; Bergan, N. E.; Shepherd, J. E. Water Catalyzed−Theoretical. *Pro. Int. Symp. on Combustion*; The Combustion Institute: Pittsburgh, PA, 1990; p 217.
(15) Bjerre, A. B.; Sørensen, E. *Ind. Eng. Chem. Res.* **1992**, *31*, 1574.
(16) Brill, T. B.; Schoppelrei, J. W.; Maiella, P. G.; Belsky, A. Expt. in Aqueous Phase. *Proc. Int. Conf. Solvothermal Reactions*; Committee of Solvothermal Technol. Res.: Takamastu, Kagawa, Japan, 1996; p 5.
(17) Tokmakov, I. V.; Hsu, C.-C.; Moskaleva, L. V.; Lin, M. C. *Mol. Phys.* **1997**, *92*, 581.
(18) Wang, B.; Hou, H.; Gu, Y. *Chem. Phys.* **1999**, *243*, 27.
(19) Akiya, N.; Savage, P. E. *AIChE J.* **1998**, *44*, 405.

(20) Cammi, R.; Mennucci, B.; Tomasi, J. *J. Phys. Chem. A* **2000**, *104*, 5631.
(21) Cossi, M.; Scalmani, G.; Rega, N.; Barone, V. *J. Chem. Phys.* **2002**, *117*, 43.
(22) Becke, A. D. *J. Chem. Phys.* **1992**, *96*, 2155.
(23) Becke, A. D. *J. Chem. Phys.* **1992**, *97*, 9173.
(24) Becke, A. D. *J. Chem. Phys.* **1993**, *98*, 564.
(25) Mebel, A. M.; Morokuma, K.; Lin, M. C. *J. Chem. Phys.* **1995**, *103*, 7414.
(26) Frisch, M. J.; et al. *Gaussian 03*, revision C.01; Gaussian, Inc.: Wallingford, CT, 2004.
(27) Bjarnov, E.; Hocking, W. H. *Z. Naturforsch., A: Phys. Sci.* **1978**, *33*, 610.
(28) Miyazawa, T.; Pitzer, K. S. *J. Chem. Phys.* **1959**, *30*, 1076.
(29) Klippenstein, S. J. *J. Chem. Phys.* **1992**, *96*, 367.
(30) Klippenstein, S. J.; Marcus, R. A. *J. Chem. Phys.* **1987**, *87*, 3410.
(31) Wardlaw, D. M.; Marcus, R. A. *Chem. Phys. Lett.* **1984**, *110*, 230.
(32) Wardlaw, D. M.; Marcus, R. A. *J. Chem. Phys.* **1985**, *83*, 3462.
(33) Mokrushin, W.; Bedanov, V.; Tsang, W.; Zachariah, M.; Knyazev, V. *ChemRate, version 1.5.2*; National Institute of Standards and Technology: Gaithersburg, MD, 2006.
(34) Saito, K.; Shiose, T.; Takahashi, O.; Hidaka, Y.; Aiba, F.; Tabayashi, K. *J. Phys. Chem. A* **2005**, *109*, 5352.

JP801247D